La Matematica
https://doi.org/10.1007/s44007-024-00093-2

ORIGINAL RESEARCH ARTICLE

Asymptotic Errors in the Superconvergence of Discontinuous Galerkin Methods Based on Upwind-Biased Fluxes for 1D Linear Hyperbolic Equations

Tianshi Lu[1] · Sirvan Rahmati[1]

Received: 19 July 2022 / Revised: 26 December 2023 / Accepted: 1 February 2024

Abstract

In this paper, we study the superconvergence of the semi-discrete discontinuous Galerkin (DG) method for linear hyperbolic equations in one spatial dimension. The asymptotic errors in cell averages, downwind point values, and the postprocessed solution are derived for the initial discretization by Gaussian projection (for periodic boundary condition) or Cao projection Cao et al. (SIAM J. Numer. Anal. **5**, 2555–2573 (2014)) (for Dirichlet boundary condition). We proved that the error constant in the superconvergence of order $2k+1$ for DG methods based on upwind-biased fluxes depends on the parity of the order k. The asymptotic errors are demonstrated by various numerical experiments for scalar and vector hyperbolic equations.

Keywords Superconvergence · Discontinuous Galerkin · Postprocessing · Upwind-biased flux · Asymptotic error

1 Introduction

Discontinuous Galerkin (DG) method is a class of finite element methods that uses discontinuous piecewise polynomials of order up to k as test functions. The DG scheme is used widely for solving linear and nonlinear partial differential equations. Reed and Hill [26] introduced the DG method for solving a steady-state linear hyperbolic equation in 1973. Cockburn et al. [13–16] applied it to time-dependent nonlinear conservation laws.

In the past two decades, various superconvergence properties of DG methods have been studied, which provided a deeper understanding of DG solutions. According to the error in the DG method, the superconvergence divides into the following three

✉ Tianshi Lu
tianshi.lu@wichita.edu

[1] Mathematics & Statistics, Wichita State University, 1845 Fairmount, Wichita, KS 67260-0033, USA

Published online: 19 March 2024

categories. The first category is superconvergence of the error in cell average and at Radau points, measured in the discrete L_2 norm (see, e.g., [2–4]). The second category is the superconvergence of the DG solution toward a particular projection of the exact solution, called the supercloseness, typically measured in the standard L_2 norm. Some of the results are available in [6, 8, 10, 12, 23, 28]. The last category is the superconvergence of the postprocessed solution. Negative-order norm estimates are a standard tool to derive superconvergent error estimates of the postprocessed solution in the L_2 norm. The choice of negative-order norms is to detect the oscillatory behavior of a function around zero. Postprocessing aims to obtain a better approximation by convolving the numerical solution by a local averaging operator. For more information, we refer the reader to [7, 17, 20, 21, 25].

Now we shall review some of the superconvergence results and some of the relevant methods used in our work. Adjerid et al. [5] was first to show that the DG solution is superconvergent at Radau points for solving ordinary differential equations and steady-state hyperbolic problems. Later, Yang and Shu in [28] studied superconvergence properties of the DG method for linear hyperbolic equations and proved that with suitable initial discretization, the error between the DG solution and the exact solution is $(k + 2)$th-order superconvergent at the downwind-biased Radau points. Around the same time, Guo, Zhong, Qiu [19] used the Fourier approach and decomposed the error. They symbolically computed eigenvalues and the corresponding eigenvectors of the DG method for low-order approximations. Shortly after, Cao, Zhang, and Zou [8] showed that if the initial discretization is close enough to a particular reconstructed function, then the $(2k + 1)$th (or $(2k + 1/2)$th) superconvergence rate at the downwind points as well as the domain average is achieved. Meng, Shu, and Wu [24] introduced the upwind-biased flux and showed the optimal a priori error estimates of order $k + 1$. Cao et al. [9] proved the $(2k + 1)$th-order superconvergence of the cell-averaged numerical solution obtained with the initial discretization by a special global projection. Most studies have concentrated on the order of accuracy and neglected the role that the error coefficient plays in the estimates. Recently, Frean and Ryan [18] used a similar approach and showed that the semi-discrete error has dissipation errors of order $2k + 1$ and $2k + 2$ order of dispersion. For upwind-biased fluxes, they showed the critical role of the error constant in the dispersion and dissipation error for approximation polynomial degree k, where $k = 0, 1, 2, 3$.

Cao showed the $(2k + 1)$ order of convergence in Ref. [8] for the first time, using the correction function technique. The idea of this technique is to construct a suitable correction function to correct the error between the exact solution and its Radau projection. Many papers have used this technique to show the semi-discrete DG method's superconvergence for one-dimensional problems. One of the recent papers done by Xu, Meng, Shu, Zhang [27] uses a slightly modified correction function and the L_2-norm stability to establish the superconvergence property of the Runge–Kutta discontinuous Galerkin method for solving a linear constant-coefficient hyperbolic equation. They show that under a $r + 1$ temporal and $2k + 2$ spatial smoothness assumption, and by choosing a specific initialization, the cell average and the numerical flux are $\min(2k+1, r)$ superconvergent. They also proved a similar result for the postprocessed solution, even if the initialization is the L_2 or Gauss-Radau projection.

Besides the Fourier analysis and the correction function technique, Padé approximation is another standard method for analyzing the DG method's superconvergence. Krivodonova and Qiu [22] used Padé approximation to analyze the spectrum of the DG method when applied to the hyperbolic equation. They showed that for a uniform computational mesh of N elements, the eigenvalues could be classified into N physical modes and kN nonphysical modes. They also show a $2k+2$ order of accuracy for the physical eigenvalue approximation. Later Chalmers and Krivodonova [11] used Padé approximation to show the $(k+2)$'th rate of superconvergence at the downwind points. They also proved that the L_2 projection of the numerical solution onto the n'th Legendre polynomial is $2k+1-n$ accurate under certain initial conditions.

Fourier analysis and the correction function technique have been widely used to study the superconvergence of the numerical errors, yet the asymptotic error has not been given explicitly. The derivation of the asymptotic error can show the connection between Fourier analysis and the correction function technique and clarify the effect of the initial discretization.

The remainder of this paper is organized as follows. In Sect. 2, we study the superconvergence of the DG methods with the upwind flux for linear hyperbolic equations with periodic boundary condition. We use Fourier analysis to derive the asymptotic errors for initial discretization by Gaussian projection, both in cell average, at downwind point, and in the postprocessed solution. In Sect. 3, we extend the analysis to DG methods with upwind-biased fluxes, which can be used to solve a system of linear hyperbolic equations using Lax-Friedrichs flux. We show that the asymptotic error depends on the parity of the order. In Sect. 4, we compute the error for linear hyperbolic equation with Dirichlet boundary condition, with initial discretization by Cao projection. The results are illustrated numerically in Sect. 5, including examples on nonlinear problems and nonuniform grids. Finally, conclusions and thoughts on future work are discussed in Sect. 6. For pedagogical purpose, an alternative proof on the accuracy of the eigenvalues and eigenfunctions for upwind-biased flux is included in the Appendix.

2 DG With the Upwind Flux

In this section,we investigate the superconvergence of the DG method with the upwind flux for the one-dimensional scalar linear hyperbolic equation with the periodic boundary condition.

2.1 Preliminary

The linear hyperbolic equation with the periodic boundary condition is

$$\begin{aligned} &u_t + u_x = 0, \quad (x,t) \in [0, 2\pi] \times [0, T]. \\ &u(x,0) = g(x), \quad u(0,t) = u(2\pi, t). \end{aligned} \tag{1}$$

We solve the equation using k'th-order DG method with the upwind flux on a uniform grid of N cells with cell size h. The numerical solution $u_h \in V_h = \{v : v|_{\tau_j} \in \mathbb{P}_k(\tau_j), 1 \le j \le N\}$, in which $\tau_j = [x_{j-1/2}, x_{j+1/2}] = [x_j - h/2, x_j + h/2]$. The equation for u_h is

$$\sum_{j=1}^{N}(v, (u_h)_t)_j = \sum_{j=1}^{N}(v_x, u_h)_j + \sum_{j=1}^{N}[[v]](x_{j+\frac{1}{2}})u_h^-(x_{j+\frac{1}{2}}), \quad \forall v \in V_h, \tag{2}$$

where $(v, u)_j = \int_{\tau_j} vudx$, $[[v]] = v^+ - v^-$, and $v^+(2\pi) = v^+(0)$. Here v^- and v^+ represent the left and right limits of v at the point, and u_h^- represents the left limit of u_h at the point. The initial discretization $u_h(x, 0)$ is a projection of $g(x)$ onto V_h. The simplest projection is the Gaussian projection, denoted by $u_G(x, t) = P_G u(x, t)$, defined by

$$(v, P_G u)_j = (v, u)_j, \quad \forall v \in \mathbb{P}_k(\tau_j). \tag{3}$$

Cao [8] introduced a special interpolation, denoted by P_I,

$$u_I(x, t) = P_I u(x, t) = u_G(x, t) + w(x, t) \equiv u_G(x, t) + \sum_{i=0}^{k} w_i(x, t), \tag{4}$$

where $w_0 = P_h^- u - P_G u$ with P_h^- being the Gauss-Radau projection, which is defined by

$$(v, P_h^- u)_j = (v, u)_j, \quad \forall v \in \mathbb{P}_{k-1}(\tau_j); \quad P_h^- u(x_{j+1/2}) = u^-(x_{j+1/2}), \tag{5}$$

and for $1 \le i \le k$, $1 \le j \le N$,

$$(v, \partial_t w_{i-1})_j = (v_x, w_i)_j, \quad \forall v \in \mathbb{P}_k(\tau_j); \quad w_i^-(x_{j+1/2}) = 0. \tag{6}$$

Notice the w_i's defined here are the opposite of those defined in Ref. [8]. We denote the solution to Eq. (2) by $u_h(x, t) = \mathcal{S}_t u_h(x, 0)$, and the projection onto piecewise constant functions in V_h by P_0. Cao [8] showed that $w_i = O(h^{k+1+i})$, and

$$\sum_{j=1}^{N}(v, (u_I - w_k)_t)_j = \sum_{j=1}^{N}(v_x, u_I)_j + \sum_{j=1}^{N}[[v]](x_{j+\frac{1}{2}})u_I^-(x_{j+\frac{1}{2}}), \quad \forall v \in V_h. \tag{7}$$

Consequently,

$$\|\mathcal{S}_t u_I(x, 0) - u_I(x, t)\|_0 \lesssim h^{2k+1}\|g\|_{2k+2}, \tag{8}$$

where $\|g\|_n$ is the norm of g in H_n, and $A \lesssim B$ implies that A is bounded by B multiplied by a constant independent of the mesh size h. Since $\|u_I(x, t) - u(x, t)\|_0 =$

$O(h^{k+1})$, the numerical solution with initial discretization $u_I(x,0)$ has $(k+1)$th-order error. However, since $\|P_0(u_I(x,t)-u(x,t))\|_0 = O(h^{2k+1})$, the cell average error,

$$e_c(x,t) = P_0(\mathcal{S}_t u_I(x,0) - u(x,t)), \tag{9}$$

is of order $2k+1$. Also, $u_I - u$ vanishes at downwind points $x^-_{j+1/2}$, so the error at downwind points is of order $2k+1$ for the initial discretization by $u_I(x,0)$. Numerical solutions of order $2k+1$ can be reconstructed from the cell averages or interpolation from the downwind point values, on a stencil of at least $2k+1$ cells. Alternatively, a smooth numerical solution can be obtained by applying a smoothness-increasing accuracy-conserving (SIAC) filter [18] to the numerical solution.

The projection u_I is not easy to compute, especially for the upwind-biased flux. We will show that for the periodic boundary condition, an initial discretization by the Gaussian projection also leads to $(2k+1)$th-order error in cell averages and at downwind points of the numerical solution, as well as the filtered numerical solution. Throughout the paper, we adopt the following notation. For any function $f(x)$ on $[0,2\pi]$, we can express $f(x)$ as the modal expansion,

$$f(x) = \sum_{j=1}^{N}\sum_{n=0}^{\infty}(f)_{j,n}\phi_{j,n}(x), \tag{10}$$

where $\phi_{j,n}(x) = \phi_n(2(x-x_j)/h)$ restricted to τ_j, in which ϕ_n is the n'th-order Legendre polynomial [1].

2.2 Asymptotic Errors for Initialization by Gaussian Projection

Theorem 2.1 *For the numerical solution to Eq.* (2) *with $u_h(x,0) = u_G(x,0)$, denote by $e_c(x,t)$ the cell average error*

$$e_c(x,t) = P_0(\mathcal{S}_t u_G(x,0) - u(x,t)), \tag{11}$$

and by $e_d(x,t)$ the error at the downwind point $x^-_{j+1/2}$ for $x \in \tau_j$. Assume $g \in H_{2k+2}$. For any fixed $t > 0$,

$$\lim_{h\to 0}\frac{e_c(x,t)}{h^{2k+1}} = (-1)^k C_k[tg^{(2k+2)}(x-t) - kg^{(2k+1)}(x-t)], \tag{12}$$

$$\lim_{h\to 0}\frac{e_d(x,t)}{h^{2k+1}} = (-1)^k C_k[tg^{(2k+2)}(x-t) - (k+1)g^{(2k+1)}(x-t)], \tag{13}$$

where

$$C_k = \frac{(k+1)!k!}{(2k+2)!(2k+1)!}. \tag{14}$$

Proof Since $u_h \in V_h$ and V_h has modal basis $\phi_{j,n}$ with $1 \le j \le N$ and $0 \le n \le k$, Eq. (2) is a linear system of ODE's for u_h expanded in the modal basis, denoted by $(u_h)_t = \mathcal{L}u_h$. By the definition of Gauss-Radau projection in Eq. (5),

$$\begin{aligned}(w_0)_{j,k} = (u - P_G u)(x^-_{j+1/2}) &= \sum_{n=k+1}^{\infty} \frac{2n+1}{h} \int_{\tau_j} \phi_{j,n}(x) g(x-t) dx \\ &= \frac{2k+3}{h} \int_{\tau_j} \phi_{j,k+1}(x) g^{(k+1)}(x_j - t) \frac{(x-x_j)^{k+1}}{(k+1)!} dx + o(h^{k+1}) \\ &= \frac{2k+3}{2} \frac{h^{k+1}}{2^{k+1}(k+1)!} g^{(k+1)}(x_j - t) \int_{-1}^{1} \phi_{k+1}(y) y^{k+1} dy + o(h^{k+1}) \\ &= \frac{(k+1)!}{(2k+2)!} g^{(k+1)}(x_j - t) h^{k+1} + o(h^{k+1}).\end{aligned} \tag{15}$$

where we used the identity $\int_{\tau_j} \phi^2_{j,n}(x)dx = h/(2n+1)$. By Eq. (6) and the identity

$$\int_{-1}^{1} \phi_n'(y)\phi_i(y)dy = 1 - (-1)^{n-i}, \quad 0 \le i < n, \tag{16}$$

we have

$$(w_n)_{j,k-n} = \frac{h}{2(2(k-n+1)+1)} \partial_t (w_{n-1})_{j,k-n+1}, \quad 1 \le n \le k. \tag{17}$$

In particular,

$$\partial_t (w_k)_{j,0} = (-1)^{k+1} C_k g^{(2k+2)}(x_j - t) h^{2k+1} + o(h^{2k+1}). \tag{18}$$

where C_k is given by Eq. (14). Since $w = \sum_{n=0}^{k} w_n$,

$$(w)_{j,n} = (-1)^{k-n} \frac{(k+1)!k!(2n+1)!}{(2k+2)!(2k+1)!n!} g^{(2k+1-n)}(x_j - t) h^{2k+1-n} + o(h^{2k+1-n}), \quad 0 \le n \le k. \tag{19}$$

Eq. (7) can be written as $(u_I)_t = \mathcal{L}u_I + (w_k)_t$, which gives

$$\begin{aligned}u_I(x,t) - \mathcal{S}_t u_I(x,0) &= \int_0^t \mathcal{S}_{t-\tau} \partial_t (w_k)(x,\tau) d\tau \\ &= (-1)^{k+1} C_k t g^{(2k+2)}(x-t) h^{2k+1} + o(h^{2k+1}).\end{aligned} \tag{20}$$

The cell average error of $u_I(x,t)$ is

$$P_0(u_I(x,t) - u(x,t)) = (w)_{j,0} = (-1)^k C_k g^{(2k+1)}(x-t) h^{2k+1} + o(h^{2k+1}). \tag{21}$$

So the cell average error in the numerical solution with initial discretization by $u_I(x,0)$ is

$$P_0(\mathcal{S}_t u_I(x,0) - u(x,t)) = (-1)^k C_k [t g^{(2k+2)}(x-t) + g^{(2k+1)}(x-t)] h^{2k+1} + o(h^{2k+1}). \tag{22}$$

For the initial discretization by Gaussian projection, we use the Fourier analysis. It has been shown in Ref. [11] that eigenvalues of $\mathcal{L}$ consist of N physical modes,

$$\lambda_0^{(m)} = -im + O(m^{2k+2} h^{2k+1}), \tag{23}$$

and kN nonphysical modes,

$$\lambda_n^{(m)} = -\frac{\alpha_n}{h} + O(m), \quad 1 \le n \le k, \tag{24}$$

with $-\lfloor \frac{N-1}{2} \rfloor \le m \le \lfloor \frac{N}{2} \rfloor$. For the nonphysical modes, $\Re\alpha_n > 0$, so only physical modes appear in the asymptotic solutions. The error due to the initial discretization by the Gaussian projection is

$$\begin{aligned}
&\mathcal{S}_t u_I(x,0) - \mathcal{S}_t u_G(x,0)\\
&= \sum_{m=-\lfloor \frac{N-1}{2} \rfloor}^{\lfloor \frac{N}{2} \rfloor} e^{im(x-t)} \frac{1}{2\pi} \int_0^{2\pi} e^{-imx} w(x,0) dx + o(h^{2k+1})\\
&= \sum_{m=-\lfloor \frac{N-1}{2} \rfloor}^{\lfloor \frac{N}{2} \rfloor} e^{im(x-t)} \sum_{n=0}^{k} \sum_{j=1}^{N} (-1)^{k-n} C_k\\
&\quad \frac{(2n+1)!}{n!} g^{(2k+1-n)}(x_j) h^{2k+1-n} \int_0^{2\pi} \frac{e^{-imx}}{2\pi} \phi_{j,n}(x) dx + o(h^{2k+1})\\
&= \sum_{m=-\lfloor \frac{N-1}{2} \rfloor}^{\lfloor \frac{N}{2} \rfloor} e^{im(x-t)} \sum_{n=0}^{k} \sum_{j=1}^{N} (-1)^{k-n} C_k \frac{(2n+1)!}{n!} g^{(2k+1-n)}(x_j) h^{2k+1-n}\\
&\quad \frac{h}{2\pi} \frac{n!(-imh)^n}{(2n+1)!} e^{-imx_j} + o(h^{2k+1})\\
&= (-1)^k C_k h^{2k+1} \sum_{n=0}^{k} \sum_{m=-\lfloor \frac{N-1}{2} \rfloor}^{\lfloor \frac{N}{2} \rfloor} e^{im(x-t)} \frac{1}{2\pi} \int_0^{2\pi} (im)^n g^{(2k+1-n)}(x) e^{-imx} dx + o(h^{2k+1})\\
&= (-1)^k C_k h^{2k+1} \sum_{n=0}^{k} \sum_{m=-\infty}^{\infty} e^{im(x-t)} \frac{1}{2\pi} \int_0^{2\pi} g^{(2k+1)}(x) e^{-imx} dx + o(h^{2k+1})\\
&= (-1)^k C_k h^{2k+1} (k+1) g^{(2k+1)}(x-t) + o(h^{2k+1}).
\end{aligned} \tag{25}$$

Here we used the fact that the Fourier series of $g^{(2k+1)}$ converges because $g \in H^{2k+2}$. Combining the two errors in Eqs.(22) and (25), we get Eq. (12). Since $u_I - u$ vanishes at downwind points, Eq. (13) follows from Eqs.(20) and (25). □

The error of the numerical solution $\mathcal{S}_t u_G(x,0)$ is asymptotically of order $2k+1$ only in the cell average and at the downwind points for a fixed time $t > 0$. The actual error is only of order $k+1$ because it has large oscillations. We can reconstruct numerical solutions of order $2k+1$ from the cell averages or the solution at downwind points, on a stencil of at least $2k+1$ cells. On a stencil of at least $2k+3$ cells, the reconstruction error is of order higher than $2k+1$, so the asymptotic errors at any point in the reconstructed solutions are given by Eqs.(12) and (13), respectively. Alternatively, to filter out the oscillations, we can postprocess the numerical solution, as introduced by Cockburn et al. [17]. The postprocessed solution for the numerical solution $u_h(x,t)$ is

$$K_h^{2s+2,k+1}(x)\star u_h(x,t) = \sum_{j=-s}^{s} c_j \psi_h^{(k+1)}(x-jh)\star u_h(x,t), \tag{26}$$

where $\psi_h^{(k+1)}(x)$ is the B-spline function of order $k+1$ on the grid with cell width h, and the number c_i are chosen to make $K_h^{2s+2,k+1}$ reproduces polynomials in P_{2s+1} by convolution. The value s for the stencil is at least k. Numerical experiments show that $s = k+1$ generates significantly smaller errors than $s = k$. Bramble and Schatz [7] related the postprocessed error to the negative-order norm of the divided differences of the original error, and Cockburn et al. [17] used it to prove that the postprocessed error has order $2k+1$ everywhere for any time $t \in [0, T]$. We will derive the asymptotic error of the postprocessed solution in the following theorem.

Theorem 2.2 *Let the postprocessed solution of $\mathcal{S}_t u_G(x,0)$ be*

$$u_K(x,t) = K_h^{2s+2,k+1}(x)\star\mathcal{S}_t u_G(x,0), \quad s \geq k. \tag{27}$$

Assume $g \in H_{2k+2}$. For any $t \in [0, T]$ with T being a fixed positive number,

$$\lim_{h\to 0} \frac{u_K(x,t) - u(x,t)}{h^{2k+1}} = (-1)^k C_k t g^{(2k+2)}(x-t), \tag{28}$$

where C_k is defined in Eq. (14).

Proof Since $K_h^{2s+2,k+1}$ reproduces polynomials in P_{2s+1} by convolution, $K_h^{2s+2,k+1}\star u(x,t) - u(x,t) = o(h^{2s+1}) = o(h^{2k+1})$, and so

$$u_K(x,t) - u(x,t) = K_h^{2s+2,k+1}\star(\mathcal{S}_t u_G(x,0) - u(x,t)) + o(h^{2k+1}). \tag{29}$$

It has been shown in [17] that all nonphysical modes are suppressed by the filter $\psi_h^{(k+1)}$. The filter $K_h^{2s+2,k+1}$ only retains the physical part, i.e., the projection onto the physical modes. In other words,

$$K_h^{2s+2,k+1}\star(\mathcal{S}_t u_G(x,0) - u(x,t))$$

$$= \sum_{m=-\lfloor \frac{N-1}{2} \rfloor}^{\lfloor \frac{N}{2} \rfloor} \frac{e^{imx}}{2\pi}$$

$$\int_0^{2\pi} e^{-imx}(\mathcal{S}_t u_G(x,0) - u(x,t))dx + o(h^{2k+1}). \tag{30}$$

The error can be decomposed into

$$\begin{aligned} \mathcal{S}_t u_G(x,0) - u(x,t) &= \mathcal{S}_t u_G(x,0) - u_I(x,t) \\ &+ u_I(x,t) - u_G(x,t) + u_G(x,t) - u(x,t). \end{aligned} \tag{31}$$

By Eqs. (20) and (25),

$$\begin{aligned} &K_h^{2s+2,k+1} \star (\mathcal{S}_t u_G(x,0) - u_I(x,t)) \\ &= (-1)^k C_k[tg^{(2k+2)}(x-t) - (k+1)g^{(2k+1)}(x-t)]h^{2k+1} + o(h^{2k+1}). \end{aligned} \tag{32}$$

Since $u_I(x,t) - u_G(x,t) = w(x,t)$, by similar procedures as in Eq. (25), we see that

$$\begin{aligned} &K_h^{2s+2,k+1} \star (u_I(x,t) - u_G(x,t)) \\ &= (-1)^k C_k(k+1)g^{(2k+1)}(x-t)h^{2k+1} + o(h^{2k+1}). \end{aligned} \tag{33}$$

The physical part of $u(x,t) - u_G(x,t)$ is

$$\sum_{j=1}^{N} \sum_{n=k+1}^{\infty} \phi_{j,n}(x) \frac{2n+1}{h} \int_{\tau_j} \phi_{j,n}(x) g(x-t) dx, \tag{34}$$

which is $O(h^{2k+2})$ by the arguments in Eq. (25). The sum of Eqs. (32) and (33) gives Eq. (28). $\square$

3 DG With the Upwind-Biased Flux

In this section, we solve the linear hyperbolic equation with the upwind-biased flux.

$$\sum_{j=1}^{N} (v, (u_h)_t)_j = \sum_{j=1}^{N} (v_x, u_h)_j + \sum_{j=1}^{N} [[v]](x_{j+\frac{1}{2}}) u_h^*(x_{j+\frac{1}{2}}), \quad \forall v \in V_h, \tag{35}$$

where

$$u_h^* = \frac{u_h^- + u_h^+}{2} - M \frac{u_h^+ - u_h^-}{2}, \quad M > 0. \tag{36}$$

We denote the solution to Eq. (35) by $\mathcal{S}_t^M u_h(x,0)$. In the notation of Ref. [9], $M = 2\theta - 1$ with $\theta > 1/2$. M can be any positive constant. The flux is reduced to the upwind flux when $M = 1$. For a vector linear hyperbolic equation or a nonlinear hyperbolic equation, $u_t + (f(u))_x = 0$, the DG method with an upwind-biased flux is

$$\sum_{j=1}^{N}(v,(u_h)_t)_j = \sum_{j=1}^{N}(v_x, f(u_h))_j + \sum_{j=1}^{N}[[v]](x_{j+\frac{1}{2}})F_h^*(x_{j+\frac{1}{2}}), \quad \forall v \in V_h, \tag{37}$$

where

$$F_h^* = \frac{f(u_h^-)+f(u_h^+)}{2} - M\frac{u_h^+ - u_h^-}{2}, \quad M > 0. \tag{38}$$

The upwind-biased flux is the well-known Lax-Friedrichs flux if we set M to be the local or global maximum wave speed. Frean and Ryan [18] studied the error constant for the DG method of order $k = 0, 1, 2, 3$ with the upwind-biased flux and showed the dependency on the parity of k. We will derive the asymptotic errors for arbitrary orders.

Theorem 3.1 *For the numerical solution to Eq. (35) with $u_h(x,0) = u_G(x,0)$, denote by $e_c^M(x,t)$ the cell average error,*

$$e_c^M(x,t) = P_0(\mathcal{S}_t^M u_G(x,0) - u(x,t)), \tag{39}$$

and by $e_d^M(x,t)$ the error at the downwind point $x_{j+1/2}$ for $x \in \tau_j$,

$$e_d^M(x,t) = u_h^*(x_{j+1/2},t) - u(x_{j+1/2},t). \tag{40}$$

Assume $g \in H_{2k+2}$. For any fixed $t > 0$,

$$\lim_{h\to 0}\frac{e_c^M(x,t)}{h^{2k+1}} = \chi_M(-1)^k C_k[tg^{(2k+2)}(x-t) - kg^{(2k+1)}(x-t)], \tag{41}$$

$$\lim_{h\to 0}\frac{e_d^M(x,t)}{h^{2k+1}} = \chi_M(-1)^k C_k[tg^{(2k+2)}(x-t) - (k+1)g^{(2k+1)}(x-t)], \tag{42}$$

where C_k is defined in Eq. (14), and

$$\chi_M = \begin{cases} M, & k \text{ even} \\ 1/M, & k \text{ odd} \end{cases}. \tag{43}$$

For any $t \in [0,T]$ with T being a fixed positive number, the numerical solution filtered by $K^{2s+1,k+1}$ with $s \geq k$ has the asymptotic error,

$$\lim_{h\to 0}\frac{K_h^{2s+1,k+1}(x)\star\mathcal{S}_t^M u_G(x,0) - u(x,t)}{h^{2k+1}} = \chi_M(-1)^k C_k t g^{(2k+2)}(x-t). \tag{44}$$

Proof Eq. (35) can be written as

$$\sum_{j=1}^{N}(u_t+u_x,v)_j=-\sum_{j=1}^{N}[[u]](x_{j+1/2})$$
$$\left(\frac{v^+(x_{j+1/2})+v^-(x_{j+1/2})}{2}+\frac{M}{2}[[v]](x_{j+1/2})\right),$$
$$\forall v\in V_h, \tag{45}$$

which gives the energy estimate,

$$\frac{\mathrm{d}}{\mathrm{d}t}(u,\bar{u})=-M\sum_{j=1}^{N}|[[u]](x_{j+\frac{1}{2}})|^2\le 0. \tag{46}$$

The equality holds only if $[[u]]=0$. It implies that the inequality is exact for nonconstant eigenfunctions. Therefore, nonphysical eigenvalues have negative real parts. The physical eigenfunctions can be constructed using Cao's projection P_I^M for upwind-biased fluxes [9], which is defined by

$$u_I^M(x,t)=P_I^M u(x,t)=u_G(x,t)+w^M(x,t)\equiv u_G(x,t)+\sum_{i=0}^{k}w_i^M(x,t), \tag{47}$$

where $w_0^M(x,t)=\sum_{j=1}^{N}(w_0^M)_{j,k}(t)\phi_{j,k}(x)$ such that the difference $d(x,t)=u_G(x,t)+w_0^M(x,t)-u(x,t)$ satisfies $d^*(x_{j+1/2},t)=0$ for all $1\le j\le N$. For $1\le i\le k$, $1\le j\le N$,

$$(v,\partial_t w_{i-1}^M)_j=(v_x,w_i^M)_j,\quad \forall v\in\mathbb{P}_k(\tau_j);\quad (w_i^M)^*(x_{j+1/2})=0. \tag{48}$$

The projection is global. However, we will show that the leading order terms of $w_i^M(x,t)$ are still local. Since $u\in H_{k+2}$, we have

$$d^-(x_{j+1/2})=(w_0^M)_{j,k}-u_{j,k+1}+o(h^{k+1}), \tag{49}$$

and

$$\begin{aligned}d^+(x_{j+1/2})&=(-1)^k(w_0^M)_{j+1,k}-(-1)^{k+1}u_{j+1,k+1}+o(h^{k+1})\\&=(-1)^k(w_0^M)_{j,k}-(-1)^{k+1}u_{j,k+1}+o(h^{k+1}).\end{aligned} \tag{50}$$

It's easy to verify that $d^*(x_{j+1/2},t)=0$ implies

$$(w_0^M)_{j,k}=\chi_M u_{j,k+1}+o(h^{k+1}), \tag{51}$$

where χ_M is defined by Eq. (43). Subsequently, $(w^M)_{j,n} = \chi_M w_{j,n} + o(h^{2k+1-n})$ for $0 \leq n \leq k$,

$$\begin{aligned} u_I^M(x,t) - \mathcal{S}_t^M u_I^M(x,0) &= \chi_M (-1)^{k+1} C_k t g^{(2k+2)} \\ &\quad (x-t) h^{2k+1} + o(h^{2k+1}), \qquad (52) \\ \mathcal{S}_t^M u_I^M(x,0) - \mathcal{S}_t^M u_G(x,0) &= \chi_M (-1)^k C_k (k+1) g^{(2k+1)} \\ &\quad (x-t) h^{2k+1} + o(h^{2k+1}), \qquad (53) \\ P_0(u_I^M(x,t) - u(x,t)) &= \chi_M (-1)^k C_k g^{(2k+1)} \\ &\quad (x-t) h^{2k+1} + o(h^{2k+1}). \qquad (54) \end{aligned}$$

Hence Eqs. (41) and (44). Since $(U_I^M)^*(x_{j+1/2},t) = u(x_{j+1/2},t)$, we have Eq. (42). $\square$

Applying Theorem 3.1 to $u(x,t) = e^{im(x-t)}$, we see that the m'th physical eigenfunction

$$r_0^{(m)}(x) = P_I^M e^{imx} + O(h^{2k+1}), \tag{55}$$

and the error of the m'th physical eigenvalue gives rise to $P_I^M e^{im(x-t)} - \mathcal{S}_t^M P_I^M e^{imx}$. Therefore,we obtain the following corollary.

Corollary 3.2 *The m'th physical eigenvalue of Eq. (35), the DG method with the upwind-biased flux, is*

$$\lambda_0^{(m)} = -im - \chi_M C_k m^{2k+2} h^{2k+1} + o(m^{2k+2} h^{2k+1}), \tag{56}$$

where χ_M and C_k are given in Eqs. (43) and (14), respectively. The associated eigenfunction $r_0^{(m)}(x)$ satisfies

$$\begin{aligned} \left(r_0^{(m)}(x) - e^{imx}\right)_{j,n} &= \chi_M (-1)^{k-n} C_k \\ &\quad \frac{(2n+1)!}{n!} (imh)^{2k+1-n} e^{imx_j} + o((mh)^{2k+1-n}). \qquad (57) \end{aligned}$$

For the upwind flux, Ref. [22] showed the supercloseness of the physical eigenvalues to the exact values, by proving that $R_{k,k+1}(\lambda_0^{(m)}) = \exp(imh)$, where $R_{k,k+1}(z)$ is the $[k/k+1]$ Padé approximation of $\exp(-z)$. Following Ref. [11], we can prove Corollary 3.2 by directly solving for the physical eigenvalues and eigenfunctions. The proof, though more technical, is included in the Appendix for pedagogical purpose.

4 Dirichlet Boundary

Consider the linear hyperbolic equation with Dirichlet boundary condition,

$$
\begin{aligned}
&u_t + u_x = 0, \quad (x,t) \in [0, 2\pi] \times [0, T]. \\
&u(x,0) = g(x), \quad u(0,t) = g(-t).
\end{aligned} \tag{58}
$$

The exact solution is $u(x,t) = g(x-t)$. We apply the DG method with the upwind flux,

$$
(v, (u_h)_t) = (v_x, u_h) + \sum_{j=0}^{N} [[v]](x_{j+\frac{1}{2}}) u_h^-(x_{j+\frac{1}{2}}), \quad \forall v \in V_h, \tag{59}
$$

where $v^+(2\pi) = v^-(0) = 0$, and $u_h^-(0,t) = g(-t)$. As shown in [8], the superconvergence of order $2k+1$ in cell average is retained with the initialization by P_I. The superconvergence of order $2k+1$ is lost for the initial discretization by the Gaussian projection, as explained below. Denote the solution to Eq. (59) with zero Dirichlet boundary condition by $u(x,t) = \mathcal{S}_t^D u(x,0)$. The difference between the two initial discretizations $u_G(x,0)$ and $u_I(x,0)$ is $u_G(x,0) - u_I(x,0)$, while there is no difference on the left boundary condition. For $x \in [0, 2\pi]$, the difference at later time t is $\mathcal{S}_t^D(u_G(x,0) - u_I(x,0))$, which is close to $\mathcal{S}_t v(x,0)$ solved on the extended domain $[-t, 2\pi]$ with periodic boundary condition, where $v(x,0) = u_G(x,0) - u_I(x,0)$ for $x \geq 0$ and $v(x,0) = 0$ for $x < 0$. The possible discontinuity at $x = 0$ in $v(x,0)$, $u_G(0,0) - u_I(0,0)$, causes oscillations in $\mathcal{S}_t v(x,0)$ in a few grids around $x = t$ of similar order, while $S_t v(x,0) = O(h^{2k+1})$ elsewhere. Similar conclusion applies to the initial discretization by the Radau projection. The following theorem gives the cell average error of $u_h(x,t)$ with $u_h(x,0) = u_I(x,0)$.

Theorem 4.1 *Let $u_h(x,t)$ be solution to Eq.* (59) *with $u_h(x,0) = u_I(x,0)$, and*

$$
e_c^D(x,t) = P_0(u_h(x,t) - u(x,t)). \tag{60}
$$

Assume $g \in H_{2k+2}$. For any $t \in [0, T]$ with T being a fixed positive number,

$$
\lim_{h \to 0} \frac{e_c^D(x,t)}{h^{2k+1}} = (-1)^k C_k [\min(x,t) g^{(2k+2)}(x-t) + g^{(2k+1)}(x-t)], \tag{61}
$$

where C_k is given by Eq. (14).

Proof As pointed out in [8], although the Fourier analysis doesn't apply to the Dirichlet boundary condition, the initial discretization by $u_I(x,0)$ still leads to superconvergence. The function $u_I(x,t)$ satisfies

$$\sum_{j=1}^{N}(v,(u_I-w_k)_t)_j=\sum_{j=1}^{N}(v_x,u_I)_j+\sum_{j=1}^{N}[[v]](x_{j+\frac{1}{2}})u_I^-(x_{j+\frac{1}{2}}),\quad v\in V_h, \tag{62}$$

with $u_I^-(0,t)=g(-t)$. Subtracting Eq. (59), and letting $u_{Ih}(x,t)=u_I(x,t)-u_h(x,t)$, we have

$$\sum_{j=1}^{N}(v,(u_{Ih}-w_k)_t)_j=\sum_{j=1}^{N}(v_x,u_{Ih})_j+\sum_{j=1}^{N}[[v]](x_{j+\frac{1}{2}})u_{Ih}^-(x_{j+\frac{1}{2}}),\quad v\in V_h, \tag{63}$$

with $u_{Ih}^-(0,t)=0$. So $u_{Ih}(x,t)$ solves the hyperbolic equation with zero Dirichlet boundary condition.

$$\begin{aligned}u_{Ih}(x,t)&=\int_0^t \mathcal{S}_{t-\tau}^D(w_k)_t(x,\tau)d\tau=\int_0^t (w_k)_t(x,t)I_{x>\tau}d\tau=(w_k)_t(x,t)\min(x,t)\\&=(-1)^{k+1}C_k\min(x,t)g^{(2k+2)}(x-t)h^{2k+1}+o(h^{2k+1}).\end{aligned} \tag{64}$$

Theorem 4.1 follows from Eqs.(64) and (21). □

5 Numerical Simulations

In this section,we perform several numerical experiments to demonstrate the superconvergence properties stated in the previous sections. In all examples, the time integration is done by a 5th-order Runge–Kutta scheme with the CFL number 0.1.

Example 5.1

$$\begin{aligned}&u_t(x,t)+u_x(x,t)=0,\quad (x,t)\in[0,2\pi]\times(0,1],\\&u(x,0)=\cos^5(x),\quad u(0,t)=u(2\pi,t).\\&u_h(x,0)=u_G(x,0).\end{aligned} \tag{65}$$

In the first example, we validate the asymptotic errors given in Theorem 2.1 and Theorem 2.2. Table 1 compares the L_2 norm of the errors in cell average (e_c), at downwind points (e_d), and the numerical solution filtered by $K^{2s+2,k+1}$ with $s=k$ and $s=k+1$, respectively. We also computed the L_s norm of the errors in the numerical solutions reconstructed from $2s+1$ cell averages (e_{cr}) or $2s+2$ downwind point values (e_{dr}). Table 2 compares e_{cr} and e_{dr} on stencils of $s=k$ and $s=k+1$. All errors are of order $2k+1$. The errors in the filtered or reconstructed solutions are smaller on a wider stencil due to the reduction of the interpolation error. The interpolation error also accounts for the apparent order of higher than $2k+1$ in the filtered and reconstructed solutions.

Table 1 Example 1. Error in cell averages, at downwind points, and in filtered solutions for $k = 1, 2, 3$

k	N	e_c	Order	e_d	Order	$e_K, s = k$	Order	$e_K, s = k + 1$	Order
1	40	4.18E–03	–	4.64E–03	–	4.73E–03	–	4.25E–03	–
	80	5.56E–04	2.91	6.06E–04	2.94	5.81E–04	3.03	5.47E–04	2.96
	160	7.08E–05	2.97	7.68E–05	2.98	7.12E–05	3.03	6.91E–05	2.99
	320	8.90E–06	2.99	9.65E–06	2.99	8.79E–06	3.02	8.66E–06	3.00
2	40	2.39E–05	–	2.67E–05	–	1.02E–04	–	3.13E–05	–
	80	7.84E–07	4.93	8.59E–07	4.96	2.08E–06	5.62	7.68E–07	5.35
	160	2.48E–08	4.98	2.71E–08	4.99	4.46E–08	5.55	2.31E–08	5.05
	320	7.79E–10	4.99	8.49E–10	5.00	1.06E–09	5.40	7.20E–10	5.01
3	40	1.79E–07	–	8.65E–07	–	1.42E–05	–	1.74E–06	–
	80	8.16E–10	7.78	6.04E–09	7.16	6.40E–08	7.80	2.50E–09	9.44
	160	5.12E–12	7.31	4.62E–12	10.3	2.61E–10	7.94	6.33E–12	8.63
	320	3.95E–14	7.02	4.24E–14	6.77	1.04E–12	7.97	3.96E–14	7.32

Table 2 Example 1. Error in reconstructed solutions for $k = 1, 2, 3$

k	N	$e_{cr}, s = k$	order	$e_{cr}, s = k + 1$	order	$e_{dr}, s = k$	order	$e_{dr}, s = k + 1$	order
1	40	6.31E–03	–	4.35E–03	–	5.24E–03	–	4.69E–03	–
	80	7.95E–04	2.99	5.60E–04	2.96	6.47E–04	3.02	6.07E–04	2.95
	160	9.86E–05	3.01	7.09E–05	2.98	7.95E–05	3.03	7.68E–05	2.98
	320	1.22E–05	3.01	8.90E–06	2.99	9.81E–06	3.02	9.65E–06	2.99
2	40	3.63E–04	–	5.32E–05	–	1.05E–04	–	3.48E–05	–
	80	1.20E–05	4.91	9.05E–07	5.88	2.13E–06	5.62	8.93E–07	5.28
	160	3.81E–07	4.98	2.52E–08	5.17	4.65E–08	5.52	2.72E–08	5.04
	320	1.19E–08	5.00	7.80E–10	5.01	1.14E–09	5.35	8.49E–10	5.00
3	40	4.29E–05	–	5.62E–06	–	1.06E–05	–	1.57E–06	–
	80	2.72E–07	6.85	1.27E–08	8.78	4.31E–08	7.94	5.36E–09	8.20
	160	2.99E–09	6.96	2.63E–11	8.92	1.89E–10	7.83	6.03E–12	9.80
	320	2.35E–11	6.99	6.48E–14	8.67	7.58E–13	7.96	4.35E–14	7.12

The errors at $t = 1$ for $k = 2$ are plotted in Fig. 1. Figure 1(a) plots the cell average errors and the asymptotic error given in Eq. (12). Figure 1(b) plots the errors at downwind points and the asymptotic error given in Eq. (13). Figure 1(c) plots the error of numerical solution filtered by $K^{2k+4,k+1}$ and the asymptotic error given in Eq. (28). All figures clearly demonstrated the convergence to the asymptotic errors.

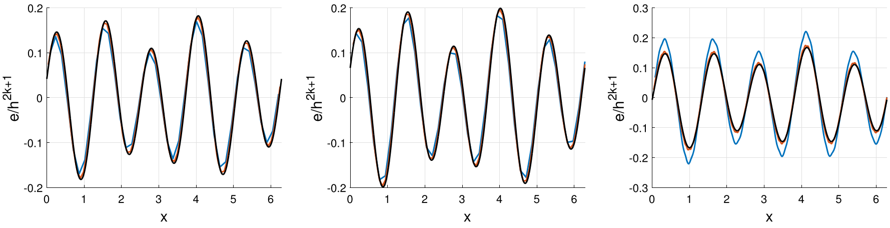

(a) e_c (b) e_d (c) e_K with $s = k + 1$

Fig. 1 Example 1. Error at $t = 1$ for $k = 2$. Blue: $N = 40$; red: $N = 80$; black: asymptotic error (color online)

Table 3 Example 2. Cell average errors for the system of linear hyperbolic equations

$k = 1$			$k = 2$			$k = 3$		
N	e_c	order	N	e_c	order	N	e_c	order
80	7.72E–02	–	40	1.10E–03	–	20	1.96E–04	–
160	9.70E–03	2.99	80	3.92E–05	4.85	40	1.57E–06	6.97
320	1.20E–03	3.00	160	1.29E–06	4.93	80	1.22E–08	7.01
640	1.52E–04	3.00	320	4.15E–08	4.95	160	1.03E–10	6.88

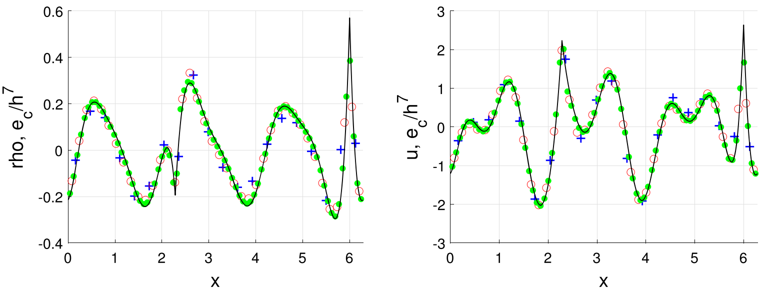

(a) e_0/h^7 for ρ (b) e_0/h^7 for u

Fig. 2 Example 2. DG solver with upwind-biased flux. The cell average error of ρ and u at $t = 1$ for $k = 3$. Crosses: $N = 20$; circles: $N = 40$; dots: $N = 80$; solid lines: asymptotic error

Example 5.2

$$
\begin{aligned}
&\rho_t + u_0\rho_x + \rho_0 u_x = 0, \quad \rho_0(u_t + u_0 u_x) + c^2\rho_x = 0, \quad (x,t) \in [0, 2\pi] \times (0, 1]; \\
&\rho(x, 0) = \sin^6(x), \\
&u(x, 0) = \left(\frac{x(2\pi - x)}{4}\right)^8; \quad \rho(0, t) = \rho(2\pi, t), \quad u(0, t) = u(2\pi, t).
\end{aligned}
\tag{66}
$$

This example uses the linearized Euler equations for isothermal gas to demonstrate the superconvergence of the DG method with the upwind-biased flux. We set $\rho_0 = 1$, $u_0 = 1$, $c = 5$, and so the two waves move with velocity 6 and -4, respectively. The

Table 4 Example 3. Cell average errors for Dirichlet boundary condition and different initial projection

k	N	Gaussian	Order	Radau	Order	Cao	Order
1	40	1.84E–03	–	1.72E–03	–	1.81E–03	–
	80	2.38E–04	2.95	2.22E–04	2.95	2.33E–04	2.96
	160	3.01E–05	2.98	2.81E–05	2.98	2.94E–05	2.99
	320	3.79E–06	2.99	3.53E–06	2.99	3.70E–06	2.99
2	40	5.17E–06	–	4.20E–06	–	4.10E–06	–
	80	2.08E–07	4.63	1.35E–07	4.96	1.31E–07	4.97
	160	1.06E–08	4.30	4.27E–09	4.98	4.11E–09	4.99
	320	7.07E–10	3.91	1.35E–10	4.98	1.29E–10	5.00
3	20	2.27E–06	–	6.81E–07	–	5.65E–07	–
	40	3.92E–08	5.86	5.65E–09	6.91	4.67E–09	6.92
	80	8.24E–10	5.57	6.25E–11	6.50	3.71E–11	6.98
	160	3.66E–11	4.49	6.70E–13	6.54	2.87E–13	7.01

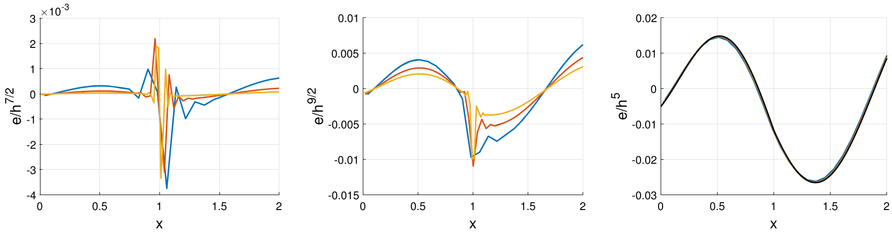

(a) Gaussian projection (b) Radau projection (c) Cao projection

Fig. 3 Example 3. Cell average error at $t = 1$ for Dirichlet boundary condition with $k = 2$ and different initial discretization. Blue: $N = 80$; Red: $N = 160$; Orange: $N = 320$; Black((c) only): asymptotic error

equation is solved using the Lax-Friedrichs flux with $M = 6$, initialized by Gaussian projection. The combined L_2 cell average error of ρ and u at $t = 1$ is listed in Table 3. It confirms the superconvergence of order $2k + 1$. It's interesting to notice that the error for $N = 640$ and $k = 1$ is close to that for $N = 20$ and $k = 3$, while the former takes 100 times longer computational time than the latter. For $k = 3$, the cell average errors of ρ and u at $t = 1$ are plotted in Fig. 2. It shows the convergence of the errors to the asymptotic cell average errors, which are computed by applying Theorem 3.1 to both left- and right-going waves.

Example 5.3

$$\begin{aligned} &u_t(x,t) + u_x(x,t) = 0, \quad (x,t) \in [0, 2\pi] \times (0, 1], \\ &u(x,0) = \sin^3(x - \pi/4), \quad u(0,t) = \sin^3(-t - \pi/4). \end{aligned} \tag{67}$$

The third example solves the hyperbolic equation with Dirichlet boundary condition. The exact solution if $u(x,t) = \sin^3(x - t - \pi/4)$. The phase factor $\pi/4$ is introduced to ensure the differences between the initial discretizations at the origin.

Table 5 Example 4. Cell average errors for a linear hyperbolic equation with nonconstant wave speed

$k = 1$			$k = 2$			$k = 3$		
N	e_c	order	N	e_c	order	N	e_c	order
40	4.48E–03	–	40	2.74E–05	–	40	2.67E–07	–
80	5.99E–04	2.90	80	9.05E–07	4.92	80	3.41E–09	6.29
160	7.64E–05	2.97	160	2.88E–08	4.98	160	1.14E–11	8.22
320	9.62E–06	2.99	320	9.04E–10	4.99	320	7.68E–14	7.21

The cell average errors at $t = 1$ for the initial discretization by Gaussian projection, Radau projection, and Cao projection are shown in Table 4. Figure 3 shows the cell average errors for $k = 2$. Figure 3 demonstrates the convergence of the error to the asymptotic form in Eq. (61).

As shown in Fig. 3, the L_∞ error for the initial discretization by Cao projection is of order $2k + 1$. For other initial projections, the errors are of order $2k + 1$ except for a few grids around $x = t$, where the error is of order $k+3/2$ for Gaussian projection and of order $k + 5/2$ for Radau projection. The L_2 errors due to the initial discretization by Gaussian and Radau projection are of order $k + 2$ or $k + 3$, respectively. It agrees with the orders in Table 4.

Example 5.4

$$\begin{aligned}
&u_t + (a(x)u)_x = s(x,t), \quad (x,t) \in [0, 2\pi] \times (0, 1],\\
&u(x,0) = \cos^5(x), \quad u(0,t) = u(2\pi, t). \qquad (68)\\
&a(x) = 1 + \cos(x)/5, \quad s(x,t) = g_t + (a(x)g)_x, \quad g(x,t) = \cos^5(x - at).
\end{aligned}$$

The source term is set to make $u(x,t) = \cos^5(x-(1+\cos(x)/5)t)$. The equation is solved using the upwind flux and initial discretization by Gaussian projection. Table 5 demonstrates that the superconvergence of order $2k+1$ also applies to linear hyperbolic equation with nonconstant wave speed, although the Fourier analysis no longer applies. The order of convergence for $k = 3$ is not close to $2k + 1$ due to the slower decay of the nonphysical modes in the numerical solutions.

Although the asymptotic errors were derived for linear equations, numerical experiments indicated that superconvergence can often be extended to nonlinear equations. Cao et al. [10] pointed out that the superconvergence is lost near the transonic point where the wave speed vanishes. Interestingly, the next example shows that for $k = 1$, the superconvergence of order $2k + 1 = 3$ is recovered near the transonic point if we use the Lax-Friedrichs flux with a fixed M or set M to be the global maximum wave speed instead of local maximum wave speed.

Table 6 Example 5. Cell average errors for a transonic Burgers equation solved with Lax-Friedrichs flux

k	N	M = local max wave speed	order	$M = 1$	order
1	80	1.02E–04	–	6.23E–05	–
	160	1.68E–05	2.60	8.74E–06	2.83
	320	2.75E–06	2.61	1.16E–06	2.92
	640	4.62E–07	2.57	1.49E–07	2.96
2	40	1.17E–05	–	1.61E–05	–
	80	6.31E–07	4.21	1.05E–06	3.94
	160	3.21E–08	4.30	7.03E–08	3.90
	320	2.14E–09	3.91	5.54E–09	3.67
3	20	5.39E–06	–	1.25E–05	–
	40	4.00E–07	3.75	2.79E–07	5.49
	80	1.94E–08	4.37	4.58E–09	5.93
	160	7.13E–10	4.77	7.69E–11	5.90

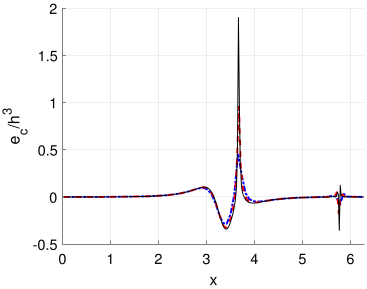

(a) M is local maximum wave speed

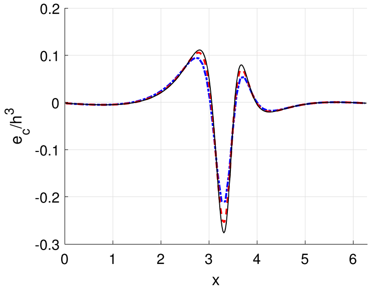

(b) $M = 1$

Fig. 4 Example 5. Cell average errors for the transonic Burgers equation solved with $k = 1$ and Lax-Friedrichs flux. Dash-dotted (blue): $N = 80$; dashed (red): $N = 160$; solid (black): $N = 320$ (Color figure online)

Example 5.5

$$
\begin{aligned}
&u_t + (\frac{u^2}{2})_x = 0, \quad (x,t) \in [0, 2\pi] \times (0, 0.5], \\
&u(x,0) = \sin(x) + \frac{1}{2}, \quad u(0,t) = u(2\pi, t). \\
&u_h(x,0) = u_G(x,0).
\end{aligned}
\tag{69}
$$

Table 6 lists the cell average errors for the transonic Burgers equation solved with the Lax-Friedrichs flux, with M being the local maximum wave speed or the constant 1. Figure 4 compares the cell average errors with $k = 1$ for the two choices of M. [10] pointed out that the $(2k + 1)$th-order superconvergence is lost around the supersonic (stagnant) points $x = 7\pi/6$ and $x = 11\pi/6$, as shown in Fig. 4(a). As a result, in Table 6, the orders of error for M being the local max wave speed are lower than

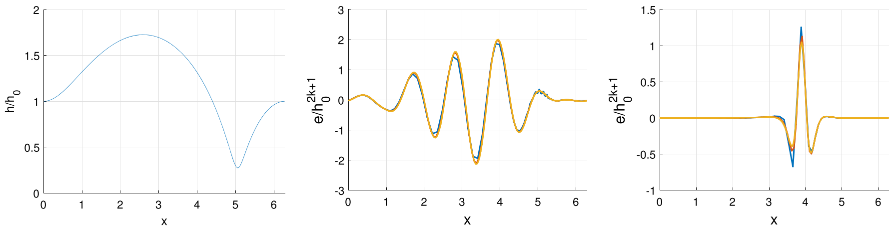

(a) Grid size distribution (b) Linear equation (c) Burgers' equation

Fig. 5 Example 6. **a** Normalized cell size distribution of the nonuniform grid. **b** Cell average error with $k = 2$ for the linear equation. **c** Cell average error with $k = 2$ for the non-transonic Burgers equation. Blue: $N = 80$; red: $N = 160$; brown: $N = 320$

$2k + 1$. However, the error with $M = 1$ in the flux are of higher orders for $k = 1$ and $k = 3$. In particular, the cell average for $k = 1$ with $M = 1$ is 3rd-order accurate. According to Theorem 3.1, the error constant for the Lax-Friedrichs flux with a fixed M is proportional to a/M for odd k, where a is the wave speed. Near the transonic points, $a = O(h)$, so the error is reduced by the factor a/M, hence the enhanced orders by setting $M = 1$ for $k = 1$ and $k = 3$. For $k = 2$, the error constant is M/a, and there is no order enhancement by setting $M = 1$, as shown in Table 6.

Example 5.6 (a)

$$\begin{aligned} &u_t(x,t) + u_x(x,t) = 0, \quad (x,t) \in [0, 2\pi] \times (0, 1], \\ &u(x, 0) = \cos^5(x), \quad u(0, t) = u(2\pi, t). \\ &u_h(x, 0) = u_G(x, 0). \end{aligned} \tag{70}$$

(b)

$$\begin{aligned} &u_t + \left(\frac{u^2}{2}\right)_x = 0, \quad (x,t) \in [0, 2\pi] \times (0, 0.5], \\ &u(x, 0) = \sin(x) + \frac{3}{2}, \quad u(0, t) = u(2\pi, t). \\ &u_h(x, 0) = u_G(x, 0). \end{aligned} \tag{71}$$

The linear hyperbolic equation and the Burgers equation are solved on a nonuniform grid using Lax-Friedrichs flux with $M = 1$. The initial condition for the Burgers equation is set to avoid transonic points, so as to achieve the $(2k + 1)$th-order superconvergence. The grid size normalized by the average grid size $h_0 = 2\pi/N$ is shown in Fig. 5. Table 7 indicates that the superconvergence of order $2k + 1$ holds on the nonuniform grid for both linear and nonlinear equations. Figure 5 shows that the cell average error has an asymptotic form that depends on the nonuniform grid.

Table 7 Example 6. Cell average errors obtained on a nonuniform grid

k	N	Linear equation	order	Burgers equation	order
1	80	1.53E–03	–	5.67E–04	–
	160	2.00E–04	2.94	8.39E–05	2.76
	320	2.53E–05	2.98	1.13E–05	2.89
	640	3.17E–06	2.99	1.47E–06	2.95
2	40	1.67E–04	–	4.88E–05	–
	80	5.89E–06	4.83	1.67E–06	4.87
	160	1.91E–07	4.95	4.62E–08	5.18
	320	6.02E–09	4.99	1.34E–09	5.11
3	40	5.57E–06	–	7.02E–07	–
	80	1.77E–07	4.97	1.64E–08	5.42
	160	3.54E–09	5.65	2.00E–10	6.35
	320	2.30E–11	7.27	1.98E–12	6.66

6 Conclusion

In this paper, we studied the superconvergence of the semi-discrete discontinuous Galerkin method for scalar and vector linear hyperbolic equations in one spatial dimension. For the periodic boundary condition, we used Fourier analysis to prove that for the initial discretization by Gaussian projection, the cell average error and error at downwind points are asymptotically of order $2k + 1$ for any fixed positive time. We showed that a numerical solution of order $2k + 1$ can be reconstructed from the cell averages or the downwind point values. We also derived the asymptotic forms of the cell average and downwind errors as well as the error of the solution obtained by a SIAC filter. Then we extended the results to DG solvers with upwind-biased fluxes and showed that the error constant depends on the parity of k. We also computed the asymptotic error in cell average for the linear hyperbolic equation with Dirichlet boundary condition. All the theoretical results presented have been validated by numerical examples. In addition to that, we presented some numerical examples of nonlinear equations and nonuniform grids.

Although the current work is on linear hyperbolic equations solved by DG method on a uniform mesh, numerical experiments showed that much of the results can be extended to more general settings. Our future work involves the analysis of superconvergence for nonlinear hyperbolic equations solved on nonuniform grids.

Funding Not applicable.

Code availability Not applicable.

Declarations

Conflict of interest The authors declare that they have no conflict of interest.

Appendix

We present a direct proof of Corollary 3.2 following the approach of Ref. [11].

Proof For $-\lfloor \frac{N-1}{2} \rfloor \leq m \leq \lfloor \frac{N}{2} \rfloor$, denote the m'th physical eigenvalue and eigenfunction of Eq. (35) by λ and $u(x)$, respectively. For any $v \in V_h(\tau_j)$, Eq. (35) can be written as

$$(u_t + u_x, v) = [[u]](x_{j-1/2}) \left(\frac{M-1}{2} v^-(x_{j+1/2}) e^{imh} - \frac{M+1}{2} v^+(x_{j-1/2}) \right). \tag{72}$$

Scaled from $x \in \tau_j$ to $y = 2(x - x_j)/h \in [-1, 1]$, the eigenfunction on $[-1, 1]$ satisfies

$$\lambda h u + 2u_y = (-1)^{k+1} [[u]] (R^M_{k+1})'(y), \quad u \in P_k, \tag{73}$$

where $[[u]] = u(-1) - u(1)e^{-imh}$, and

$$R^M_{k+1}(y) = \begin{cases} a_M \phi_{k+1}(y) - b_M \phi_k(y), & k \text{ even} \\ b_M \phi_{k+1}(y) - a_M \phi_k(y), & k \text{ odd} \end{cases}, \tag{74}$$

in which

$$a_M = e^{\frac{imh}{2}} \left(\cos \frac{mh}{2} - iM \sin \frac{mh}{2} \right), \quad b_M = e^{\frac{imh}{2}} \left(M \cos \frac{mh}{2} - i \sin \frac{mh}{2} \right). \tag{75}$$

Notice that $a_M + b_M = M + 1$, and $a_M - b_M = (1 - M)e^{imh}$. Since $u \in P_k$,

$$u(y) = [[u]] \frac{(-1)^k}{2} \sum_{l=1}^{k+1} \frac{R^{M,(l)}_{k+1}(y)}{(-\frac{\lambda h}{2})^l}. \tag{76}$$

Substituting in $y = 1$ and using the formula $\phi^{(k+1)}_{k+1} = (2k+1)!!$, we get for even k,

$$[[u]] = -(\lambda h)^{k+1} \frac{k!}{(2k+1)!} \frac{u(1)}{a_M} + O((\lambda h)^{k+2})$$

$$= -(\lambda h)^{k+1}\frac{k!}{(2k+1)!} + O((\lambda h)^{k+2}), \tag{77}$$

and for odd k,

$$\begin{aligned}[[u]] &= -(\lambda h)^{k+1}\frac{k!}{(2k+1)!}\frac{u(1)}{b_M} + O((\lambda h)^{k+2}) \\ &= -(\lambda h)^{k+1}\frac{k!}{(2k+1)!}\frac{1}{M} + O((\lambda h)^{k+2}). \end{aligned} \tag{78}$$

Multiplying Eq. (73) by $e^{\lambda h(y+1)/2}$ and integrating by parts repeatedly, we obtain

$$\begin{aligned} u(y) = &\left(u(1) - \frac{M-1}{2}[[u]]e^{imh}\right)e^{-imh-\frac{\lambda h}{2}(y+1)} + \frac{(-1)^{k+1}}{2}[[u]] \\ &\sum_{l=0}^{\infty}(-\frac{\lambda h}{2})^l R_{k+1}^{M,(-l)}(y), \end{aligned} \tag{79}$$

where $R_{k+1}^{M,0}(y) = R_{k+1}^{M}(y)$, and for $l \geq 0$,

$$R_{k+1}^{M,(-l-1)}(y) = \int_{-1}^{y} R_{k+1}^{M,(-l)}(z)dz. \tag{80}$$

Expanding in Legendre polynomials, we have

$$R_{k+1}^{M,(-l)}(y) = \sum_{i=k-l}^{k+l+1} c_i^l \phi_i(y), \quad 0 \leq l \leq k, \tag{81}$$

where

$$c_{k-l}^l = \begin{cases} (-1)^{l+1}\frac{(2k-2l+1)!!}{(2k+1)!!}b_M, & k \text{ even} \\ (-1)^{l+1}\frac{(2k-2l+1)!!}{(2k+1)!!}a_M, & k \text{ odd} \end{cases}. \tag{82}$$

In particular,

$$R_{k+1}^{M,(-l)}(1) = \begin{cases} (-1)^k(1-M)e^{imh}, & l = 0 \\ 0, & 1 \leq l \leq k \\ 2c_0^k, & l = k+1 \end{cases}. \tag{83}$$

Setting $y = 1$ in Eq. (79), we get

$$\begin{aligned} &\left(u(1) - \frac{M-1}{2}[[u]]e^{imh}\right)(1 - e^{-imh-\lambda h}) \\ &= \frac{(-1)^{k+1}}{2}[[u]]\left((-\frac{\lambda h}{2})^{k+1}2c_0^k + O((\lambda h)^{k+2})\right). \end{aligned} \tag{84}$$

Substituting in $[[u]]$, we get

$$\lambda + im = -\chi_M \frac{(k+1)!k!}{(2k+2)!(2k+1)!} m^{2k+2} h^{2k+1} + o(m^{2k+2} h^{2k+1}), \tag{85}$$

where $\chi_M = M$ for even k, and $\chi_M = 1/M$ for odd k. Normalizing u by

$$u(1) - \frac{M-1}{2}[[u]]e^{imh} = e^{\frac{imh}{2}}, \tag{86}$$

we get from Eq. (79) that

$$u(y) = e^{imhy/2} + \frac{(-1)^{k+1}}{2}[[u]] \sum_{l=0}^{k} (-\frac{\lambda h}{2})^l R_{k+1}^{M,(-l)}(y) + o((mh)^{2k+1}). \tag{87}$$

Substituting in $[[u]]$ and expressing $u(y)$ as $\sum_{n=0}^{k} u_n \phi_n(y)$, we have

$$u_n = p_n^{(m)} + (-1)^{k-n} \chi_M \frac{(k+1)!k!(2n+1)!}{(2k+2)!(2k+1)!n!} (imh)^{2k+1-n} + o((mh)^{2k+1-n}), \tag{88}$$

where $p_n^{(m)}$ is the projection of $e^{imhy/2}$ onto $\phi_n(y)$. □

References

1. Abramowitz, M., Stegun, I. (eds.): Handbook of Mathematical Functions. Dover, New York (1965)
2. Adjerid, S., Baccouch, M.: The discontinuous Galerkin method for two-dimensional hyperbolic problems. Part I: superconvergence error analysis. J. Sci. Comput. **33**, 75–113 (2007)
3. Adjerid, S., Baccouch, M.: The discontinuous Galerkin method for two-dimensional hyperbolic problems Part II: a posteriori error estimation. J. Sci. Comput. **38**, 15–49 (2009)
4. Adjerid, S., Baccouch, M.: Asymptotically exact a posteriori error estimates for a one-dimensional linear hyperbolic problem. Appl. Numer. Math. **60**, 903–914 (2010)
5. Adjerid, S., Massey, T.C.: Superconvergence of discontinuous Galerkin solutions for a nonlinear scalar hyperbolic problem. Comput. Methods Appl. Mech. Engrg. **195**, 3331–3346 (2006)
6. Baccouch, M.: Recovery-based error estimator for the discontinuous Galerkin method for nonlinear scalar conservation laws in one space dimension. J. Sci. Comput. **66**, 459–476 (2016)
7. Bramble, J.H., Schatz, A.H.: Higher order local accuracy by averaging in the finite element method. Math Comput. **31**, 94–111 (1977)
8. Cao, W., Zhang, Z., Zou, Q.: Superconvergence of discontinuous Galerkin method for linear hyperbolic equations. SIAM J. Numer. Anal. **5**, 2555–2573 (2014)
9. Cao, W., Li, D., Yang, Y., Zhang, Z.: Superconvergence of discontinuous Galerkin methods based on upwind-biased fluxes for 1D linear hyperbolic equations. ESAIM: Math. Model. Num. Anal. **51**(2), 467–486 (2017)
10. Cao, W., Shu, C.W., Yang, Y., Zhang, Y.: Superconvergence of discontinuous Galerkin method for scalar nonlinear hyperbolic equations. SIAM J. Numer. Anal. **56**(2), 732–765 (2018)
11. Chalmers, N., Krivodonova, L.: Spatial and modal superconvergence of the discontinuous Galerkin Method for linear equations. J. Sci. Comput. **72**, 128–146 (2017)
12. Cheng, Y., Shu, C.W.: Superconvergence of discontinuous Galerkin and local discontinuous Galerkin schemes for linear hyperbolic and convection-diffusion equations in one space dimension. SIAM J. **47**, 4044–4072 (2010)

13. Cockburn, B., Shu, C.W.: TVB Runge-Kutta local projection discontinuous Galerkin finite element method for conservation laws II: general framework. Math. Comp. **52**, 411–435 (1989)
14. Cockburn, B., Shu, C.W.: The Runge-Kutta discontinuous Galerkin method for conservation laws V: multidimensional systems. J. Comput. Phys. **141**, 199–224 (1998)
15. Cockburn, B., Lin, S.Y., Shu, C.W.: TVB Runge-Kutta local projection discontinuous Galerkin finite element method for conservation laws III: one dimensional systems. J. Comput. Phys. **84**, 90–113 (1989)
16. Cockburn, B., Hou, S., Shu, C.W.: The Runge-Kutta local projection discontinuous Galerkin finite element method for conservation laws IV. The multidimensional case. Math. Comp. **54**, 545–581 (1990)
17. Cockburn, B., Luskin, M., Shu, C.W., Süli, E.: Enhanced accuracy by post-processing for finite element methods for hyperbolic equations. Math. Comput. **72**, 577–606 (2003)
18. Frean, D., Ryan, J.K.: Superconvergence and the numerical flux: a study using the upwind-biased flux in discontinuous Galerkin methods. Comm. Appl. Math. and Comput. **2**, 461–486 (2020)
19. Guo, W., Zhong, X., Qiu, J.: Superconvergence of discontinuous Galerkin and local discontinuous Galerkin methods: Eigen-structure analysis based on Fourier approach. J. Comput. Phys. **235**, 458–485 (2013)
20. Ji, L., Xu, Y., Ryan, J.K.: Accuracy-enhancement of discontinuous Galerkin solutions for convection-diffusion equations in multiple-dimensions. Math. Comput. **81**, 1929–1950 (2012)
21. Ji, L., Xu, Y., Ryan, J.K.: Negative-order norm estimates for nonlinear hyperbolic conservation laws. J. Sci. Comput. **54**, 531–548 (2013)
22. Krivodonova, L., Qin, R.: An analysis of the spectrum of the discontinuous Galerkin method. Appl. Numer. Math. **64**, 1–18 (2013)
23. Meng, X., Shu, C.W., Zhang, Q., Wu, B.: Superconvergence of discontinuous Galerkin methods for scalar nonlinear conservation laws in one space dimension. SIAM J. **50**, 2336–2356 (2012)
24. Meng, X., Shu, C.W., Wu, B.: Optimal error estimates for discontinuous Galerkin methods based on upwind-biased fluxes for linear hyperbolic equations. Math. Comput. **85**(299), 1225–61 (2016)
25. Mirzaee, H., Ji, L., Ryan, J.K., Kirby, R.M.: Smoothness-Increasing Accuracy-Conserving (SIAC) postprocessing for discontinuous Galerkin solutions over structured triangular meshes. SIAM J. **49**, 1899–1920 (2011)
26. Reed, W.H., Hill, T.R.: Triangular mesh for neutron transport equation. Los Alamos Scientific Laboratory Report, **LA-UR**, 73–479 (1973)
27. Xu, Y., Meng, X., Shu, C.W., Zhang, Q.: Superconvergence analysis of the Runge-Kutta discontinuous Galerkin Methods for a linear hyperbolic equation. J. Sci. Comp. **84**, 23 (2020)
28. Yang, Y., Shu, C.W.: Analysis of optimal supercovergence of discontinuous Galerkin method for linear hyperbolic equations. SIAM J. Numer. Anal. **50**, 3110–3133 (2012)